CHAPTER 25

Microstructural Characterization and Mechanical Reliability of Laser-Machined Structures

M. Mehrpouya*, H. Lavvafi†, A. Darafsheh‡
*Sapienza University of Rome, Rome, Italy
†Loyola University Medical Center, Maywood, IL, United States
‡Washington University School of Medicine, St. Louis, MO, United States

25.1 INTRODUCTION

The need for components and devices with micron-scale dimensions and with fine structures for applications in various fields, such as electronics, medical, biomedical, aviation, microelectromechanical systems (MEMS), energy, optics, and photonics has increased rapidly in recent years [1–3]. Although traditional machining tools are widely used as a major means of fabricating such microcomponents, there still remain significant issues in the predictability and productivity of the fabrication methods, especially for microcomponents with complex shapes [4]. For instance, the trend toward miniaturization of medical devices with high-precision production has introduced new challenges for manufacturing techniques [5,6]. Surface damage during the machining process using conventional techniques can affect the performance of the machined components, especially in some specific materials that are hard to machine [7]. In addition, some designs often include fine details that are difficult to achieve with rotary tool machining. Thus, there is great interest in the use of laser microfabrication techniques.

Lasers have made possible significant advancements in cutting, welding, and many other manufacturing processes [8–16]. The ability to machine fine details with high precision, accuracy, and speed on structures made of a metal, semiconductor, ceramic, and polymer via laser ablation has paved the way for the application of laser material processing in microelectronics and other industries [16–19]. The introduction of high-power lasers with ultrashort pulses has opened a new paradigm in the laser processing of materials,

Advances in Laser Materials Processing
https://doi.org/10.1016/B978-0-08-101252-9.00025-X

allowing the creation of very high-resolution features with very little mechanical or chemical damage to the medium [12,13].

Laser micromachining requires a large amount of energy. Depending on the material and the desired machining process, different types of lasers with various power sources are used. CO_2 and Nd:YAG lasers are the most common ones used in micromachining [15]. Improvements in the quality of the cutting, drilling, and micromachining of materials through the use of lasers have enabled us to produce finer details using laser-machining compared to more conventional engraving techniques. Lasers with short pulses in the picosecond (ps) and femtosecond (fs) range have become the popular choice for micromachining because of several advantages, such as high flexibility and very small induced heat affected zones (HAZs). Femtosecond lasers can provide high-quality micromachining with minimal thermal damage because the short pulse duration results in high peak power. As a result, the material is removed by vaporization instead of melting as it occurs in long-pulse (i.e., nanosecond) or continuous laser material processing. Nanosecond lasers usually provide higher energy with a relatively lower repetition rate, generating more thermal damage than picosecond and femtosecond lasers. [20–23].

Extensive research has been done on the effects of various process parameters on the productivity of laser machining processes. An area that deserves additional attention is the effect of laser processing on the structure and mechanical properties of the laser-affected materials. A highly energetic laser beam can cause multiple phase transformations in the substrate (i.e., evaporation, deposition, melting, and solidification) as well as solid-state phase transformations, which occur due to the fast cooling rate of molten materials. The selection of laser processing variables makes a major difference in the quality of the fabricated parts and their properties.

In this chapter, we review recent developments in laser micromachining processes, which involve the integration of various micromachining processes and laser sources for improving the quality of the machining process. This chapter also deals with the mechanical characterization and reliability of laser micromachined structures.

25.2 LASER MICROMACHINING AND ITS FEATURES

Various manufacturing and material processing operations, such as laser-assisted joining, forming, machining, and surface engineering, can be performed using high-power lasers due to their ability to produce localized intense heating. Lasers are widely employed for machining, using thermal

energy to break the chemical bonds in materials. A schematic representation of a typical laser machining process is illustrated in Fig. 25.1. When a laser beam with high energy density is focused on the surface of a material, the absorbed thermal energy can transform the work volume into a molten, vaporized, or chemically changed state. A flow of a high-pressure assist gas jet is then used to accelerate and remove the transformed material from the machining zone. The parameters governing this process depend on the material properties, such as thermal conductivity, reflectivity, specific and latent heats of melting, and evaporation [25–27].

Laser machining is applicable to a variety of materials. It is a flexible, repeatable, efficient, and controlled process. Lasers can be used to process a variety of alloys as well as traditional or novel materials, such as smart alloys. To achieve a high quality of machining and maintain the original properties of the base material, the laser operating parameters such as laser power and scan speed must be carefully chosen [28–32].

An important advantage of laser processing over conventional mechanical methods is that it works with minimal contact. For example, the fabrication of cooling holes in a thermal barrier-coated superalloy requires

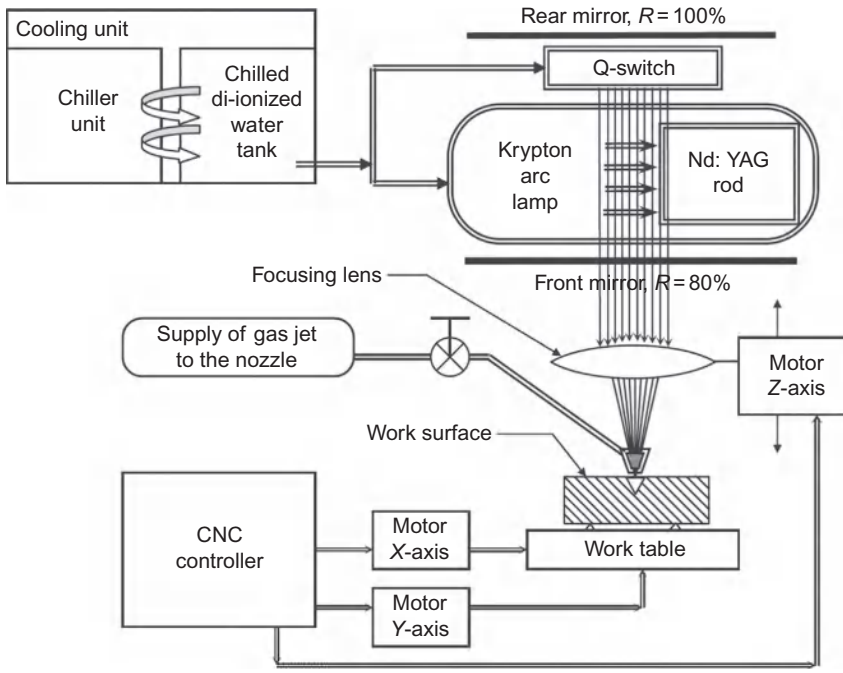

Fig. 25.1 Schematic illustration of an Nd:YAG laser machining system [24].

machining through an electrically nonconducting YSZ (yttria stabilized zirconia) layer, which is a challenging task using traditional methods such as electrodischarge and electrochemical machining. Laser machining, however, due to its noncontact nature, can be used to create such holes through melt ejection and vaporization as a result of focusing the laser beam on the surface of the material [33]. A summary of laser machining applications in several industries is tabulated in Table 25.1.

Laser micromachining has the ability to produce micron-scale structures through different methods such as direct writing, mask projection patterning, and patterning by interference of the laser beams [34,35]. The dynamics of the laser ablation process and the efficiency of laser machining depend on the optical and thermal properties of the material, such as reflectivity, absorption, and heat diffusion coefficients.

In several engineering applications, laser machining can replace the traditional mechanical material removal techniques because of its outstanding features, such as its flexibility and the fact that it is a thermal and noncontact process, as described in the following. Various material processing functions, such as welding, drilling, grooving, cutting, and heat treating can be performed by the same laser system integrated with a multiaxis positioning or robotic system. In this way, there is no need to transport the parts to specialized machines to perform each task. The ability to perform real-time monitoring of the laser processing allows online measurement of the key parameters of the sample. Hence, a high level of reproducibility can be achieved [36,37]. Due to its noncontact nature, the cutting force, tool wear, and machine vibration associated with typical mechanical methods can be eliminated in laser processing of materials because the energy transfer happens through irradiation of the material. Also, the rate of material removal is controlled by the laser processing parameters, such as laser power and processing and scanning speed, and is not affected by the maximum tool force, tool chatter, and built-up edge formation.

Fig. 25.2A shows an array of microholes drilled in a 3C–SiC wafer with a laser beam operating at a wavelength of 1040 nm with a pulse duration of 300 fs [38]. In that example, the laser beam moves along a circular path during the microlaser drilling process. Another example is shown in Fig. 25.2B for a single plate of heat exchange with microchannels used for waste heat recovery, in which the Nd:YAG nanosecond laser was used for machining while the laser beam was guided via an array of multiple mirrors inside the laser machine head. Arrows indicate the laser beam pattern that was used for micromachining [34,39].

Table 25.1 Some typical laser materials processing applications [1]

Heavy manufacturing	Light manufacturing	Electronics	Medical industry	General
Profile cutting in sheet and plate metals	Profile cutting in plastics and wood	High accuracy wire stripping	Flow orifices with <100 mm diameter	CVD diamond cutting
Seam and spot welding	Engraving	Via formation insulating material: Tab & MCM	Machining delicate or thermally sensitive materials	Ceramic and glass micromachining
Cladding and drilling	Drilling	Skiving of flexible circuits	Micromachining applications where edge quality and cleanliness are critical	Thin film patterning
		IC repair		Microlithography

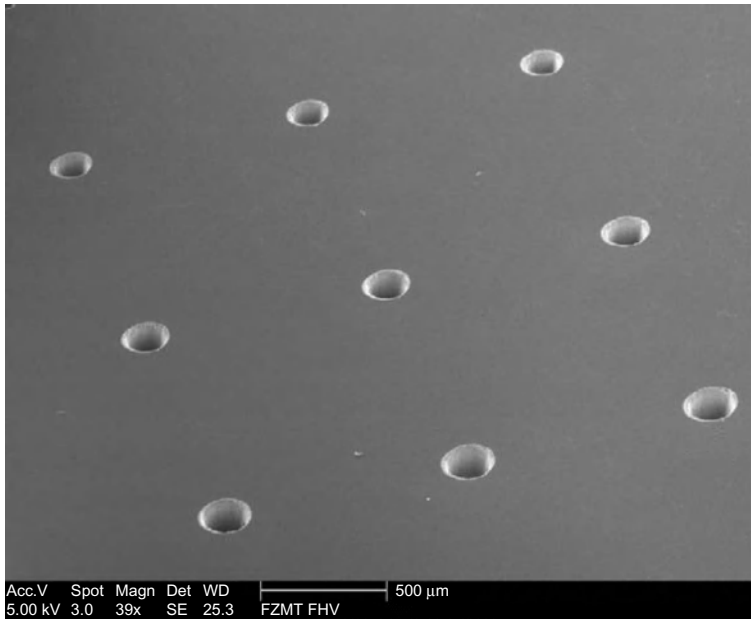

Fig. 25.2 (A) Array of microholes in a 3C–SiC wafer with 400-µm thickness drilled with a solid-state laser with a pulse duration of 300 fs at a wavelength of 1040 nm [38]. (B) Laser carving of a stainless steel plate with dimension of 15 × 50 mm, applicable as a microchannel heat exchanger with a 400-µm channel width [34].

25.3 LASER SOURCES FOR LASER MACHINING

Lasers can produce monochromatic collimated light with small (submillimeter) spot sizes, high power, narrow bandwidth, and a precisely controlled wavelength. A laser requires three fundamental components: a lasing medium, a resonator cavity, and an energy source. The lasing medium can be a

solid (glass, crystal, fiber, powder), gas (atomic, ionic, molecular, excimeric), or liquid (organic dye). The resonator cavity is basically a pair of mirrors facing each other with the lasing medium between them. The energy source, or pump, provides the energy (usually through an optical or electrical excitation) required for exciting the molecules of the lasing medium to an upper-level energy state. These molecules would spontaneously emit incoherent and poorly collimated light under normal conditions. However, in a laser, the light emission of the lasing medium is reflected within the resonator cavity such that it passes through the lasing medium multiple times, generating stimulated emission of photons from the lasing medium on each pass. Because the stimulated emission is in phase with the stimulating light field, this amplification process produces coherent and monochromatic light. One of the mirrors in the cavity is partially transmitting, so a fraction of the light amplified in the cavity is extracted on each reflection, producing a useful beam [40,41].

Different types of lasers, such as CO_2, Nd:YAG, excimer, and femtosecond lasers are used for the machining processes of various types of materials. Characteristics of typical solid-state and gas lasers, operating in deep ultraviolet (UV) to mid-infrared (IR) wavelengths, used for microfabrication are tabulated in Table 25.2.

25.3.1 Nd:YAG Lasers

Nd:YAG lasers, with a wavelength of 1.064 μm in the near-IR region of the spectrum, are the most commonly used high-power solid state lasers. The lasing medium is a crystalline matrix of yttrium-aluminum-garnet (YAG, $Y_3Al_5O_{12}$) with neodymium ions (Nd^{3+}) dopants dispersed in it. A krypton and/or xenon flash lamp serves as the energy source to excite the lasing medium.

The Nd:YAG lasers, due to their good beam quality, are able to form a very small focused beam with associated small kerf widths that make them an excellent choice for microcutting materials. In the laser beam cutting (LBC) process, the laser beam is focused on the work material and is absorbed at the cutting front. The absorbed thermal energy heats the material, transforming the prospective kerf volume into a molten, vaporized, and/or chemically changed state that can be removed by a coaxial gas jet (see Fig. 25.3) [42–47]. In addition, the slag and the oxide scales formed on the surface due to laser cutting can be removed by acid pickling using an HNO_3 bath followed by electrolysis. A smooth surface can be achieved after electrochemical polishing.

Table 25.2 Laser types used in microfabrication application [35]

Type of laser	Laser material	Wave length	Pulse length	Frequency
Solid state laser	Nd:YAG (2nd harmonic)	532 nm	100–10 ns	50 Hz
	Nd:YAG (3rd harmonic)	355 nm		
	Nd:YAG (4th harmonic)	266 nm		
	Nd:YVO_4	1064 nm	2.8–7.9 ps	84 MHz to 77 GHz
	Nd:$GDVO_4$	1053 nm	37 ps	100 MHz
	Nd:BEL	1070 nm	2.9–7.5 ps	250 MHz to 20 GHz
	Nd:LSB	1062 nm	1.6–208 ps	177–240 MHz
	Nd:glass	1054 nm	7 ps	
	Nd:VAN	750–870 nm		
	Nd:YLF	1047–1053 nm	1.5–37 ps	76 MHz to 2.85 GHz
	Yb:YAG	1030 nm	340–730 fs	35–81 MHz
	Yb:glass	1025–1082 nm	58–61 fs	112 MHz
	Yb:GdCOB	1045 nm	90 fs	100 MHz
	Yb:KGW	1037 nm	176 fs	86 MHz
	Ti:sapphire	750–880 nm	6–150 fs	15 MHz to 2 GHz
	Cr:LiSAF	800–880 nm	12–220 s	82–200 MHz
	Cr:LiCAF	800–820 nm	20–170 fs	90–95 MHz
	Cr:SGaF	830–895 nm	14–100 fs	71–119 MHz
	Cr:LiSCaF	860 nm	90 fs	140 MHz
	Cr:Forsterite	1.21–1.29 μm	14–48 fs	81–100 MHz
	Cr:YAG	1.52 μm	44–120 fs	81 MHz to 1.2 GHz
	Fiber lasers	1.064 μm	100 ns	20–25 Hz
	Diode lasers	0.8 μm		
	Microchip lasers	1.064 μm	Less than 100 ps	100 kHz
Gas laser	ArF	193 nm	5–25 ns	1–1000 Hz
	KrF	248 nm	2–60 ns	1–500 Hz
	XeCl	308 nm	1–250 ns	1–500 Hz
	XeF	351 nm	0.3–35	1–1000 Hz
	CO_2 laser	10.6 μm	200 μs	5 Hz
	Copper vapor lasers	611–578 nm	30 ns	4–20 Hz

Machining of superalloys using Nd:YAG lasers with nanosecond pulses is a fairly well-established practice in the aviation industry. However, their relatively long pulses (typically several ns) lead to the diffusion of a significant amount of thermal energy into the surrounding material during the machining process [48]. As a result, collateral damage consisting of recast

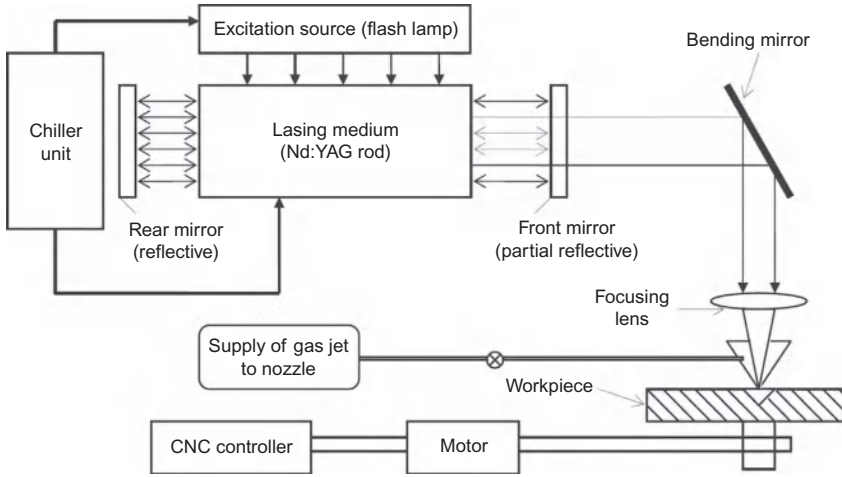

Fig. 25.3 Schematic diagram of an Nd:YAG laser beam cutting machine [42].

layer formation, melt debris, and microcracking often accompany nanosecond laser machining [33]. It should be noted that Nd:YAG fiber lasers are used in applications requiring low pulse repetition rate and high pulse energies (up to 100J/pulse), such as hole piercing and deep keyhole welding applications [7,25].

25.3.2 Carbon Dioxide Lasers

CO_2 lasers, with an output wavelength of 10.6 μm in the far-infrared (FIR) region of the spectrum, are molecular lasers, a subgroup of gas lasers. The lasing medium is a combination of carbon dioxide, nitrogen, and helium gas molecules. The excitation of the carbon dioxide is achieved by increasing the vibrational energy of the molecule through an electric discharge.

CO_2 lasers are well established in industrial processes due to their low investment costs, high reliability, and suitability for processing almost all materials. The commercial CO_2 lasers exhibit the simultaneous achievement of short pulse duration, high peak power, and high beam quality. Consequently, pulse duration is typically in the order of ms down to μs, which results in a thermal material ablation process dominated by heat conduction [49,50]. Industrial uses for CO_2 lasers include laser machining, heat treatment, and welding [7,13,25]. Compact RF-excited wave guide CO_2 lasers are well suited for micromachining processing by controlling the wave guide loss in the laser resonator [35]. The actual pumping takes place by an AC or DC electrical discharge.

25.3.3 Excimer Lasers

Excimer (short for excited dimer) lasers with the output light in the UV to near-UV range are gas lasers in which the lasing medium is a compound of two identical species that exist only in an excited state. Commonly used excimer lasers are argon fluoride (ArF), krypton fluoride (KrF), xenon chloride (XeCl), and xenon fluoride (XeF), with the output wavelengths of 193, 248, 308, and 351 nm, respectively [51]. The compound lasing medium can be formed by inducing the noble gas (Kr, Ar, or Xe) into an excited state with an electron beam, an electrical discharge, or a combination of both. Excimer lasers can be used for machining solid polymers, removing metal films from polymer substrates and micromachining ceramics and semiconductors. They are also applicable for a laser treatment process [7].

Optimizing the productivity and quality of the components manufactured using lasers is of great importance. Both aspects are influenced by the selection of appropriate laser processing parameters, such as laser wavelength and power, cutting speed, and the assist gas parameter, which depend on the material structure, thickness, desired feature size, and economic considerations. [28,29,52]. Due to their shorter wavelength, UV lasers can be focused into a smaller spot compared to the IR lasers as the focused spot size is proportional to the wavelength. Since UV light is absorbed at a shallower depth in material, a fine control of the material removal can be achieved. However, the processing rate is slower because there is less material removal per pulse. UV lasers generally have a relatively short pulse length (<100 ns), which helps to attain a high power density on the target material. The minimal thermal effect results in a good edge quality. Short wavelengths with short pulse lead to a better edge quality. However, their capital and maintenance cost is much higher. UV lasers are best used when small feature sizes and good quality are more important than the cost [9].

IR lasers have relatively longer pulses (microseconds to milliseconds) and wavelengths compared to the UV lasers. Due to their long wavelength, the laser light absorption occurs far into the material. IR lasers are available in very high output powers up to tens of kilowatts and their cost is lower than the UV lasers.

25.3.4 Femtosecond Lasers

Most of the time, machining with a nanosecond laser generates considerable damage, such as recast layer, spatter, HAZs, and in the case of having a coated substrate, delamination of the ceramic coating [22,33,53]. Even pulses in the picosecond range may lead to an unacceptable distortion of medical devices

with fine and intricate geometries. Thus, in order to produce microcomponents free of distortion, the pulse duration has to be further reduced by several orders of magnitude down to the femtosecond domain [54,55]. Recent studies have shown that the abovementioned damages to the work material can be minimized by using femtosecond lasers because the very high peak intensities achieved as a result of short pulse duration lead to the material removal by vaporization, instead of melting as in long-pulse or continuous laser material processing.

Femtosecond lasers offer a new paradigm in machining quality with high spatial resolution, minimal thermal damage, and minimal heat diffusion into the machined area periphery, which leaves behind a small amount of molten material. This small HAZ contains a low level of thermal defects, common in ns-laser processing, such as cracking and chipping [20,56]. For example, laser-machined holes with a surface roughness of less than 2 μm and with no major collateral damage have been produced by femtosecond lasers [33,34]. One reason for the reduced damage is the decreased thermal penetration depth associated with shorter pulses, as schematically illustrated in Fig. 25.4 [58–60].

Due to minimal thermal and mechanical influences in femtosecond lasers, the major effect that limits the resolution of fabricated features using such lasers is the diffraction of light waves. Structures with diffraction-limited dimensions can be readily generated in the far field. The diffraction limit can be overcome using near field material processing techniques, such as by combining a femtosecond-pulse laser with a scanning near-field

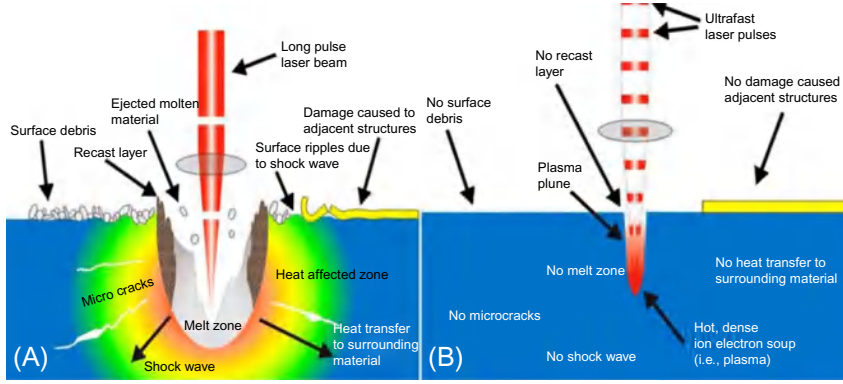

Fig. 25.4 Comparison of (A) nanosecond vs. (B) femtosecond laser ablation processes. Femtosecond lasers provide a smaller HAZ, more precise machining, and minimal collateral damage compared with their nanosecond laser counterparts [57].

optical microscope probe. In this way, the size of the generated structures is not limited by either the wavelength of laser light or thermal effects [61,62].

Sometimes there is a need to machine a variety of fine features in biomedical devices, such as in cardiovascular stents. One example is laser machining a NiTi (nitinol) cylinder with different wall thicknesses [63]. Fig. 25.5 exhibits a Nitinol stent machined by an ultrafast fiber laser. Clean, precise, straight cuts can be made in a single pass at 40 μJ pulse energy on target, 800 fs pulse duration, and 100 kHz repetition rate. The outer diameter of the tube is 3 mm with a 254-μm wall thickness [64–66].

It should be mentioned that femtosecond lasers require complicated optical devices and demanding maintenance. They also generate great scattering effects that deteriorate metal ablation [12,21,23].

25.4 METHODS OF MICROSTRUCTURE AND SURFACE EVALUATION

There are several methods practically used to evaluate the microstructure and surface characteristics of laser-machined components. These methods include but are not limited to optical microscopy (wide field and laser scanning confocal microscopy), scanning electron microcopy (SEM), transmission electron microscopy (TEM), and focused ion beam (FIB).

25.4.1 Optical Microscopy

Optical microscopy, which is a nondestructive and real-time imaging technique, is one of the most powerful and versatile investigation techniques in material sciences. The far-field spatial resolution of any standard lens-based

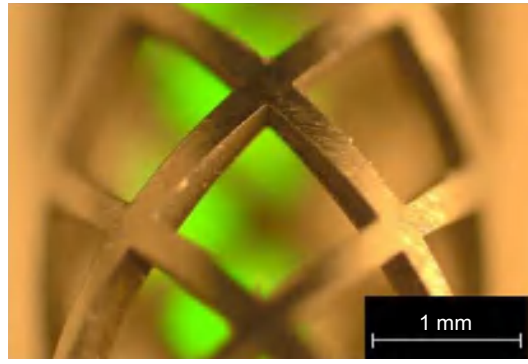

Fig. 25.5 Visible light microscope image of a nitinol stent machined with an ultrafast fiber laser [64].

optical microscope is limited by the wavelength of imaging light (λ) and by the numerical aperture (NA) of the lens system due to the diffraction of light waves. NA is defined by $NA = n \times \sin\theta$, in which n is the refractive index of the object-space medium and θ is the half-angle of the maximum cone of light that can enter (exit) the lens. For conventional white-light microscope systems, Abbe's diffraction-limit is $0.5\lambda/NA \sim 250$ nm. Confocal microscopes, benefiting from illumination and detection through pinholes, offer improvement in resolution as well as the ability to perform surface evaluation analysis. It should be noted that a variety of optical microscopy techniques based on near-field scanning probes and microscale lenses have been devised in recent years to overcome the diffraction limit. However, design complexity, slow acquisition time, and limited field of view have impeded their use to some extent [67–70].

Laser treatment will affect the surface properties of the materials. Usually when these effects are in the order of several microns, they can be readily characterized using conventional optical microscopy. Fig. 25.6A shows a cross-section of a 316LVM wire machined by using an Nd:YAG laser. The grained surface is restructured after thermal treatment as well as as-received material. Fig. 25.6B illustrates the microstructural change within the recast layer of a laser treated H13 tool steel, etched with 2% nital, in which regions of recast and HAZs are visible [34,71].

Fig. 25.6 (A) Schematic of the laser-machined wire representing the large central core and the outer skin of harder/softer material. Schematic also shows the typical grain structure in the core similar to that of as-received material. The surface grains are re-structured by the laser treatment [34]. (B) Optical micrographs showing a microstructural change, such as dissolving carbides within recast layer, for H13 tool steel laser treated and etched with 2% nital showing regions of recast, HAZ, and parent metal [34].

25.4.2 SEM, TEM, and FIB

Scanning electron microscopy, transmission electron microscopy, and focused ion beam are the imaging techniques with nanometer and subnanometer scale resolution that are particularly used in the fields of semiconductor and materials science for site-specific analysis, deposition, and ablation of materials.

An SEM uses a focused beam of electrons to image the specimen in a vacuum chamber. A focused ion beam setup is similar to a scanning electron microscope setup; however, it uses a focused beam of ions. As an example of using FIB in order to investigate the nature of recast layer produced by the laser treating, FIB can be used to make a cross-section of the laser-treated specimens. In this approach, ion beam (Ga^+) assisted Pt deposition is used as a protection layer for subsequent milling for the cross-section. Fig. 25.7 shows the steps to make a cross-section of the laser-treated sample within the recast layer induced by an Nd:YAG laser [34].

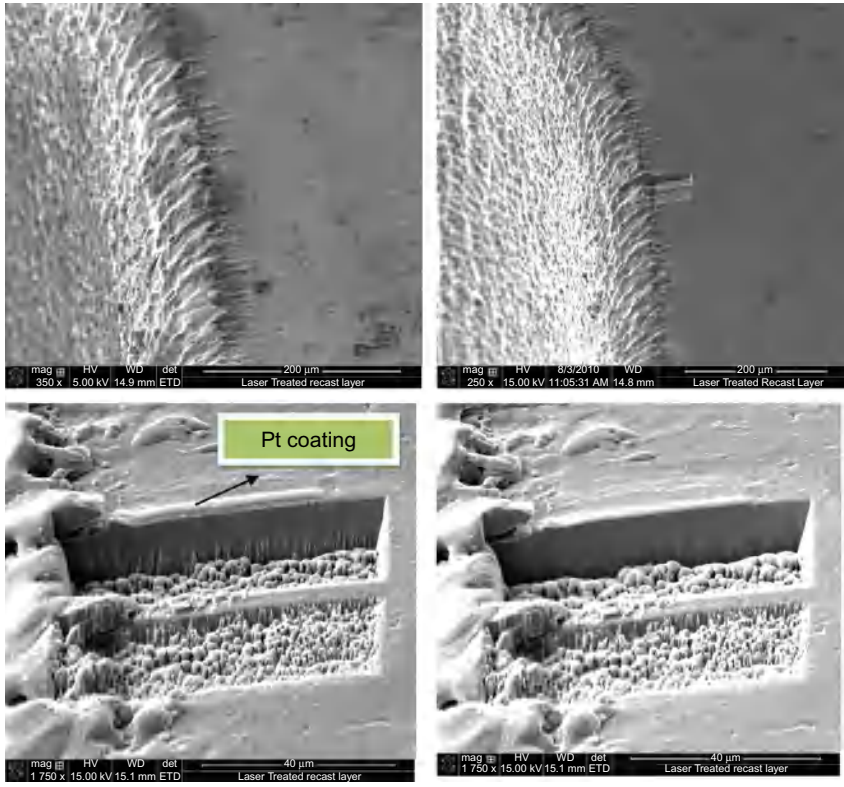

Fig. 25.7 Cross-sections showing the process of using FIB milling to study the HAZs and recast layer induced by laser treatment [34].

An example of using SEM has been presented in the following. The nitinol biliary stent can be successfully fabricated with a rounded shape and smooth edges in a precise dimension, clean surface morphology, no recast layer, and minimal HAZ produced by femtosecond laser micromachining. The SEM images of nitinol biliary stent by femtosecond laser with Type 5 path is shown in Fig. 25.8. The track of the laser beam can readily be observed in Fig. 25.8A using SEM. The surface morphology of the stent is still clean with no recast layer, and minimal HAZ is observed. The side view of the stent with Type 5 path is shown in Fig. 25.8B. As an aside, Fig. 25.8 indicates that the dimension precision of nitinol biliary stents can be significantly increased, with the structures becoming stronger and the manufacturing procedure shortened by the femtosecond laser as well [65].

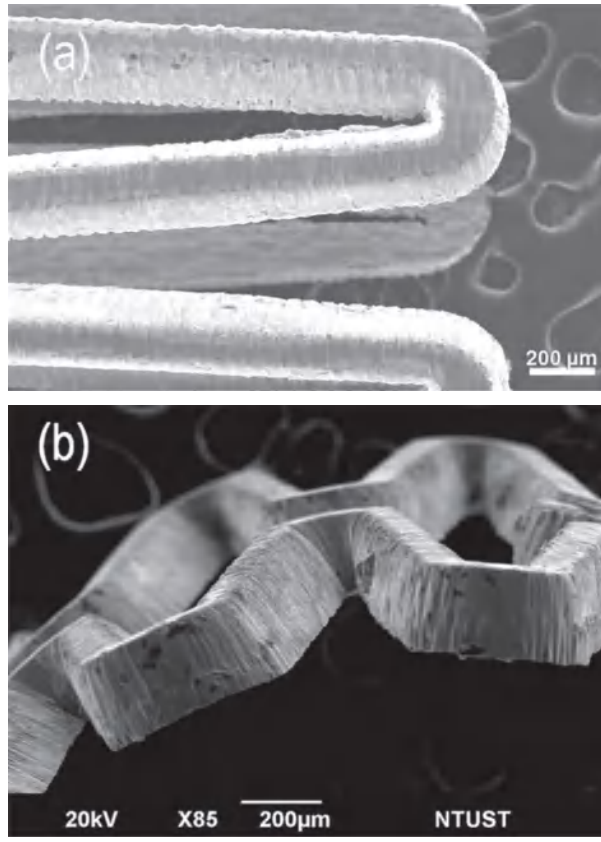

Fig. 25.8 SEM images of Nitinol biliary stent with Type 5 path: (A) top view (B) side view [65].

25.5 MECHANICAL CHARACTERISTICS AND LASER-INDUCED THERMAL EFFECTS

In the laser machining process, typically the laser beam is scanned over the target area creating the desired localized heating. During the laser-matter interaction, a very small layer of molten material is formed. The vapor plumes, formed by material vaporization, exercise an overpressure on the molten material. This results in the movement of the molten material toward the impact's edges. Fig. 25.9 demonstrates a schematic of laser processing by a fiber laser, which leads to melting a layer on the base material. The penetration depth in the melting region is schematically illustrated. One of the complications associated with laser processing is the creation of HAZs, which contain several types of undesirable effects such as distortion, surface cracking, embrittlement, decrease in weldability, and decrease in materials strength and corrosion resistance as well as reduced fatigue life. Sometimes the material properties in HAZs can be altered from the parent material, such as the creation of a resolidified material on the surface of the work material. In the subsequent sections we will discuss these issues in more detail.

25.5.1 Heat-Affected Zone

One of the difficulties in laser processing is the removal of the HAZs, such as resolidified material formed on the surface of the work material. The cooling rate in the resolidification zone significantly affects the microstructure of materials across the cross-section generated by the laser process. The laser parameters, including power and scanning speed, determine the

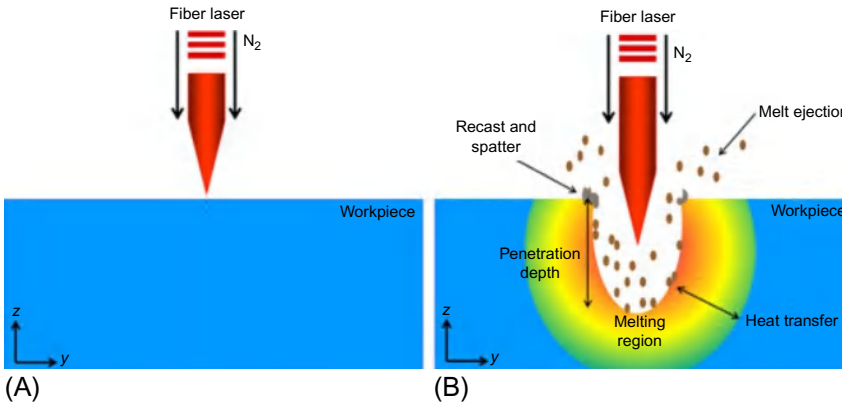

Fig. 25.9 The schematic of physical process in laser micromachining and drilling process with a static beam, (A) initial arrangement (B) after partial penetration [72].

microstructure of the materials after laser processing; it can be generally obtained from the adequate time-temperature transformation (TTT) diagrams [73]. In addition to resolidification and phase transformations, diffusion also plays an important role in defining the final metallurgical properties of laser-processed materials. The metallurgy of laser treated/machined material is highly dependent on local diffusion processes that in turn are driven by thermal and chemical gradients [73]. The function loss due to the HAZ can be minimized if a processing technique is designed to minimize the thickness of the HAZ, and the recast layers are removed after the process through various post-processing techniques. Ongoing studies have been carried out on various materials to reduce the HAZ with ultrafast lasers, such as femtosecond and picosecond lasers [74–76].

Thermal effects at the surface of the cutting kerf can lead to the alteration of the microstructure and/or mechanical properties of the laser-processed materials. It results in the formation of a distinct HAZ at the surface of the cutting edge that can be revealed by appropriate polishing and etching techniques. Hence, laser cutting parameters, such as laser power and scan speed, should be carefully chosen to minimize the heat-affected areas. Fig. 25.10 shows a typical HAZ in an Incoloy 800 HT superalloy sheet formed during laser cutting. Generally, the HAZ can be minimized by increasing the speed of the laser cutting process since higher cutting speeds reduce the heat transfer to the material [32,34,77,78].

The quality of the machining cannot be easily predicted due to the dynamic nature of the laser machining process. The cutting of ferrous alloys is an example illustrating the unpredictability of the laser cut quality. The

Fig. 25.10 Differential Interference Contrast micrograph showing the microstructural changes of a laser machined Incoloy 800 HT superalloy etched with marbles [34].

oxidation reactions with iron and other elements in the alloy add another source of heat, in addition to the laser beam itself, that causes the material removal to occur on two moving and often interacting fronts, the oxidation front and the laser beam front [52]. Striation (periodic lines appearing on the cut surface) affects the surface roughness, appearance, and geometrical precision of the products cut by laser and is an important quality factor in evaluating the laser cutting outcome [79]. Kerf width, surface roughness, and the size of the HAZ are often used to quantify laser cut quality. Fig. 25.11 illustrates the influence of the machining speed on the HAZ of XC42-steel sample. Fig. 25.11 shows that the heat-affected region decreased considerably with increasing the scan speed when the laser power remained constant ($P = 1000$W) [52].

Traditional laser manufacturing processes employ nanosecond and picosecond pulsed lasers to machine intricate designs of nitinol (NiTi) based cylindrical slugs. The significant drawback of the nanosecond and picosecond lasers is that they impart a significant amount of heat to the stent during machining. This leads to the creation of heat-affected areas including slag and recast, which should be removed with costly, labor-intensive post-processing steps such as electropolishing. Furthermore, these clean-up steps often involve the use of hazardous chemicals [63]. The fine features common in implantable and *ex vivo* medical devices require a manufacturing tool that can precisely machine micron-scale features without introducing significant heat to the rest of the workpiece. HAZs compromise device integrity, cause lower yields, and increase costly post-processing steps. Continuous wave lasers ablate through a thermodynamic process: localized heating of the target

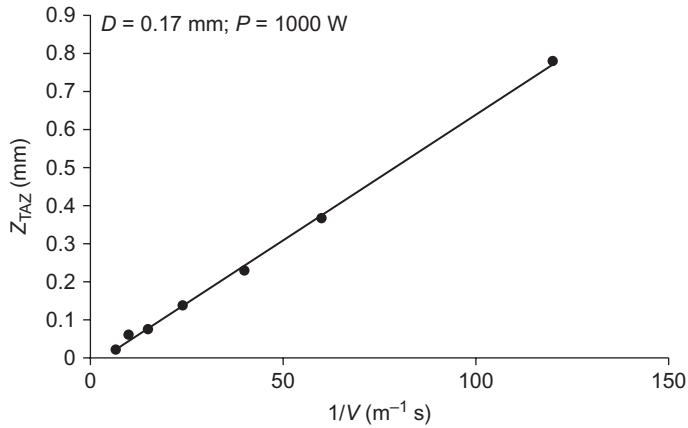

Fig. 25.11 Influence of machining speed on the HAZ [52].

lattice followed by phase change or combustion [63]. The minimization of thermal effects is also a significant consideration in the laser processing of polymers and other temperature-sensitive materials. SEM images of stents micromachined by using a continuous-wave laser and a femtosecond laser are shown in Fig. 25.12A and B, respectively. Fig. 25.12A shows a stent machined by using a continuous-wave CO_2 laser in which indiscrete edges, melting, and other thermal effects suggestive of large HAZs are observed. When the stent is placed in the arteries, the melted features, burrs, cracks, and other defects induced during the laser micromachining may lead to the failure of the device due to the complicated cyclic fatigue loading [81]. Fig. 25.12B shows a stent with smooth and fine edges machined by using a femtosecond laser. It has been shown that materials processed using ultrashort pulse lasers show fewer thermal effects; for example, an absence of burrs was noted in microscale features processed using a femtosecond laser [61,80,82–84].

25.5.2 Hardness and Flexural Strength

Studies of the mechanical properties of laser-machined materials have shown that the strength of such materials, characterized by the hardness and flexural strength, is affected by the thermal-affected zones and crack formation [85,86]. For example, it has been shown that the mean values of flexural strength of some laser-machined ceramics can be reduced to ~40% of that prior to laser machining [87]. Laser micromachining of silicon wafers has shown that the breaking limit after laser cutting will be reduced [88]. It has also been shown that the hardness of a titanium alloy sheet in HAZs is increased by ~10% after laser cutting [89].

The surface hardness is generally affected in some alloys subjected to laser treatment. For instance, surface microhardness of Nd:YAG laser-treated AISI 316LVM stainless steel was found to increase in the annealed wires, while the surface microhardness of Nd:YAG laser-treated hard wires decreased [48]. Since the laser primarily affects the surface properties of the materials, it does not measurably affect the smooth tension data or the tensile fracture surfaces, due to the relatively small affected cross-section. It is reported that the increased surface hardness of the laser-treated annealed stainless steel delays the crack initiation period, increasing a fatigue life in both low cycle fatigue (LCF) and high cycle fatigue (HCF) regimes [48].

Since the generation of a HAZ in laser micromachining is similar to the HAZ caused by other processes, such as laser welding, it is beneficial to point out some of the observations in hardness variation during

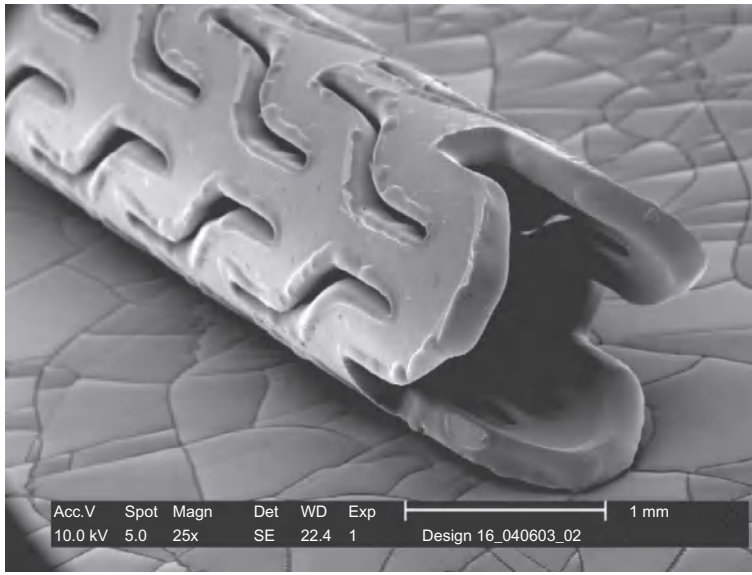

(A)

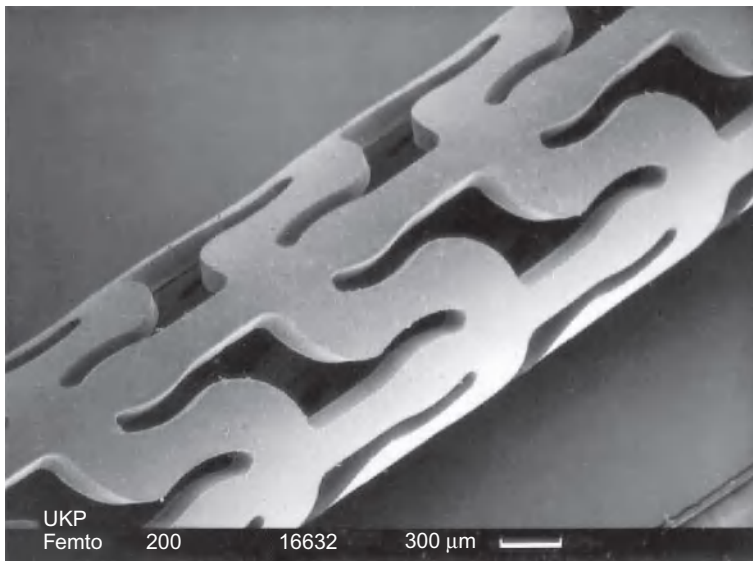

(B)

Fig. 25.12 (A) Poly(L-lactide) stent machined using a continuous-wave CO_2 laser. (B) Poly(L-lactide) stent machined using a femtosecond laser [61,80].

laser welding where the laser heat has altered the hardness of materials. Fig. 25.13 represents the hardness values of the cross-section of the welded steel CPW 800 sheets with a 2.5-mm thickness (150×300 mm). The hardness measurements are performed on the cross-section of the

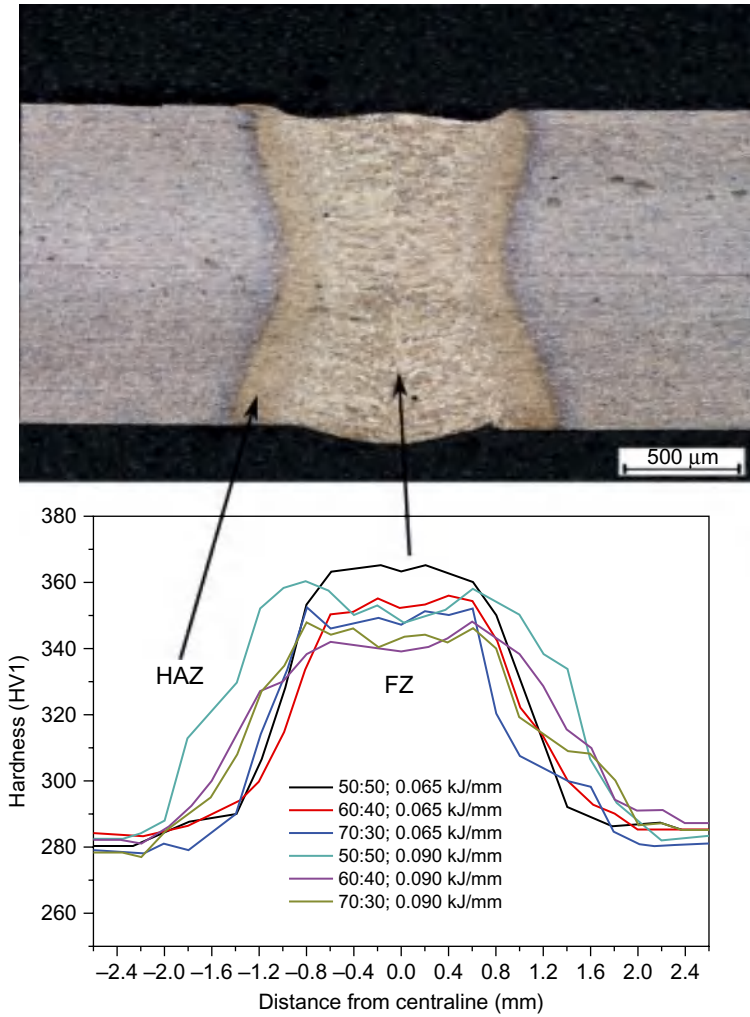

Fig. 25.13 Results of hardness measurements for various welding parameters [90].

weld in order to determine the quality of the welded joints. The highest hardness (i.e., 365 HV1) was found in the joint welded with a linear energy of 0.065 kJ/mm and a beam power distribution of 50:50. The lowest hardness (i.e., 340 HV1) was observed in the joint welded using a linear energy of 0.09 kJ/mm and a beam power distribution of 60:40. Increasing the linear energy of the weld decreased the hardness in relation to the same beam power distribution but with lower welding energy. It was concluded that the power distribution between the first and second beam affected the hardness of the welded joint [90–93].

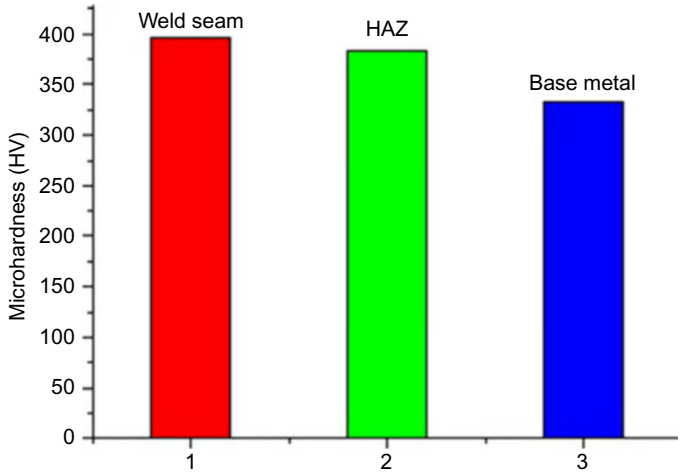

Fig. 25.14 Microhardness distribution from the welded seam to the base metal [94].

Fig. 25.14 shows the microhardness distribution of the transverse of a welded seam. It is shown that the highest hardness was found in the welded seam, at about an average of HV397. HV384 was the hardness of HAZ, and then sharply transitioned into the base metal, at a hardness of about HV333 [94].

25.5.3 Fatigue

Fatigue of materials, which is progressive and localized structural damage, refers to the gradual weakening of a material as a result of frequent loading and unloading [95]. In materials subjected to cyclic loading, when the loads are above a certain threshold, microscopic cracks begin to form at the stress concentrators. As a crack reaches a critical size, it will suddenly propagate and may cause catastrophic failure. Fatigue life is defined as the number of specified stress cycles that a specimen can tolerate before failure of a specified nature occurs.

As mentioned before, thermal damage and crack formation affect the strength of the machined components [89]. Surface roughness induced during laser machining with high power settings and/or lasers with longer pulse width (i.e., ns) results in more surface imperfections and consequently considerable loss in fatigue life. Conversely, low-energy finishing conditions with a low power setting and/or lasers with a shorter pulse width (i.e., fs and ps) introduce fewer damages to the laser-machined components. Fatigue specimens machined at different energies exhibit similar fatigue

failure mechanisms, which begin by initiating fatigue cracks at multiple locations within the surface defects in the recast layer or the HAZs [34,96]. It has been shown that under pull-push loading with a stress ratio of −1 and alternating stress with a magnitude of 0.6 UTS in the tool steel, fatigue cracks typically propagate into only a very small portion of the fracture surface before the overload fracture occurs due to fracture of the primary carbides and ductile microvoid fracture of the remaining matrix [96].

An example of fatigue studies of laser-machined wires is presented in the following where the fracture surfaces of the laser-treated 316LVM display several types of fracture surface features, depending on the number of cycles to failure (Nf). Fig. 25.15 is the SEM image of a 316LVM annealed wire machined with a femtosecond laser, fractured in flex bending fatigue after 4819 cycles. Fatigue fracture initiation is evident at the top and bottom of Fig. 25.15A. Fig. 25.15B shows a higher magnification view of fatigue striation-like features [34].

It should be mentioned that most machined materials entail stress-raising notches and other stress concentrators, such as persistent slip bands and grain interfaces that increase the nominal stress from cyclic loading. The specification and geometry of critical crack length is an important factor in controlling the fatigue behavior of the laser-machined materials where the

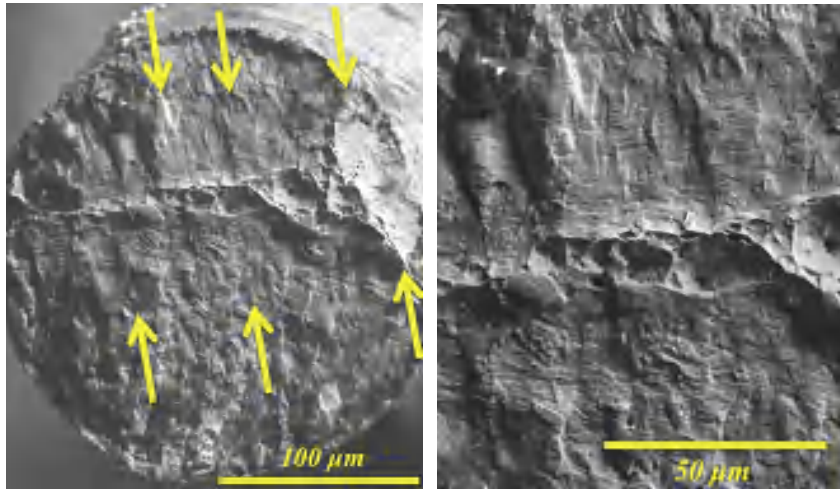

Fig. 25.15 (A) SEM image of 316LVM annealed machined with femtosecond laser, fractured in flex bending fatigue after 4819 cycles. Crack growth direction is top-to-bottom and bottom-to-top. (B) Higher magnification of (A) [34].

fatigue life is strongly dependent on the surface characteristics of a material. Sustained efforts have been made to derive fatigue computation methods applicable to different engineering applications [97,98].

25.5.4 Cracks

The laser-ablated materials are often removed from the workpiece by vaporization and/or melt ejection mechanisms during laser machining [99]. However, the melted part that is not removed from the workpiece is resolidified and forms a recast layer on the side walls and at the bottom of the cavity. The recast layer is usually brittle and acts as a nucleation site for cracking [89,99–102]. Process optimization and modeling studies are needed to reduce the recast layers produced during laser machining. Furthermore, cracks can be formed during laser processing due to other phenomena, such as phase transformation within the recast layer. If the laser causes the crystalline phase transformation, it can cause distortion as there is a mismatch in thermal properties of the resolidified layer (i.e., recast layer) and the parent materials. For example, in the recast layers of stainless steel, the microstructure is composed of a columnar structure of austenitic dendrites with minor phase of delta-ferrite in the interdendritic regions, grown epitaxial from the base material. The formation of such microstructural changes is due to rapid solidification as illustrated in Fig. 25.16 [99,103]. Energy-dispersive x-ray spectroscopy results showed that the most oxide layer found on the surface layer was produced when using oxygen as the assist gas, followed by that using argon and nitrogen [104].

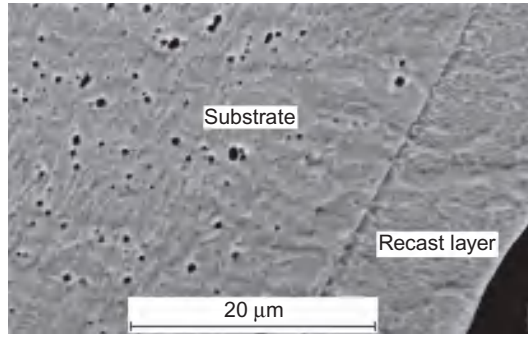

Fig. 25.16 Typical cross-section SEM image of laser-drilled type 305 stainless steel sheet showing the microstructure of the substrate and the recast layer when O_2 is used as the assist gas [99].

When the laser-machined components are designed to work in a liquid environment, it is important to make sure that the chemical and electrochemical corrosion properties of such components are appropriate based on the working environmental conditions.

Fig. 25.17 shows a cross-sectional SEM of a piece of laser-machined 316LVM by an Nd:YAG laser with nanosecond pulse and high power, which can cause multiple cracks within the recast layer. If such a piece is subjected to fatigue testing, these cracks can initiate the failure. Under scanning electron microscope inspection, the regions affected by laser micromachining revealed deep craters, higher surface roughness resulting from the melting, and solidification during the laser melting and cooling process. SEM exams of the surface affected by the laser show the presence of cracks, typical of thermally induced cracking within a recast layer as can be seen in Fig. 25.17. Microcracks are initiated at the surface of the recast layer and propagated toward the substrate. Fatigue cracks propagate into the brittle recast layer rapidly, but crack growth slows down once it gets to the tougher

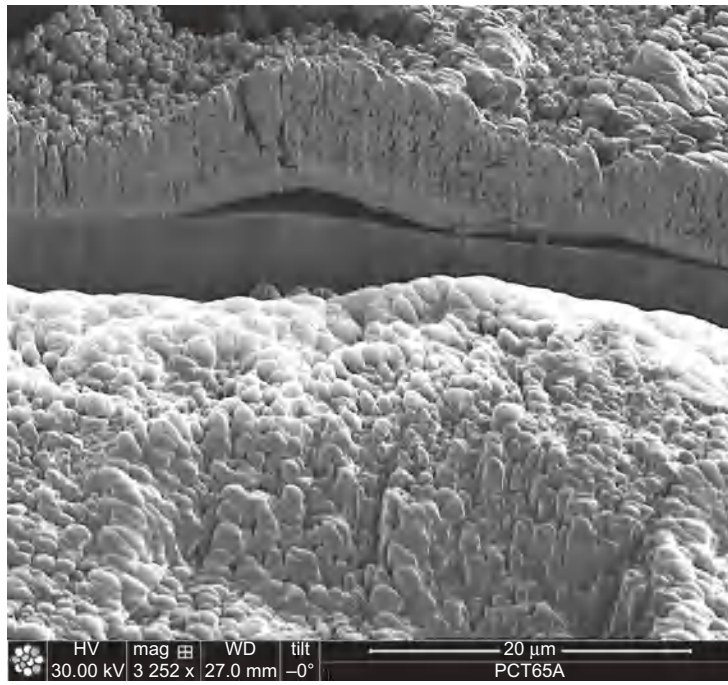

Fig. 25.17 Cross-section SEM micrograph of the laser-machined 316LVM by Nd:YAG laser. Grains of several micrometers ($2.23\,\mu m \pm 0.34\,\mu m$) are observed by ion-induced secondary electron imaging [34].

parent alloy. Once sufficient cracks approach and get to the critical length, rapid fracture occurs in the remaining cross-section [48,96].

Crack formation can be minimized by using lasers with a shorter pulse width. Compared with nanosecond and continuous wave lasers, picosecond and femtosecond laser-machined materials suffer from fewer thermal effects, such as microcrack formation. An example of a hole-array and a pin-array machined on Ti-6Al-4V material by using the ps Lumera laser (RAPID) at 100 kHz, is demonstrated in Fig. 25.18. The microholes made through both percussion and trepanning drillings showed good circularity and sharp edge. No thermal damaged zones, resolidification layers, or microcracks were found on the drilled holes. The relative orientation between the holes/pins was in agreement with the design. Also, no microcracks or recast layers were observed on the sidewalls of the machined structure [21,105].

25.6 SUMMARY

Laser micromachining plays a key role in the manufacturing of small devices, which is especially important for medical device and implant applications such as cardiovascular stents, guide wires, and needles. Laser micromachining has been extensively researched and developed to overcome the challenges in manufacturing where the traditional machining does not work due to its limitations. One of the principle advantages of laser micromachining is its great potential to provide localized material effect for the manufacturing of miniature devices. However, the thermal effect of the laser machining process may reduce surface quality and accordingly the fatigue strength due to the generated HAZ, which deteriorates the

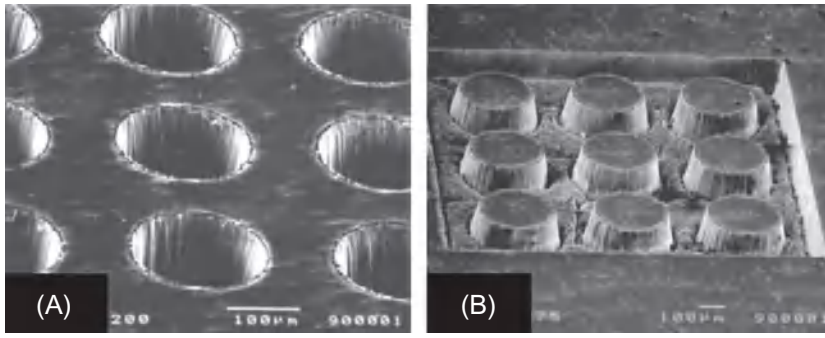

Fig. 25.18 (A) Array of holes with 175 μm diameter and 75 μm depth. (B) Array of pins with 250 μm diameter and 100 μm height [21].

performance of micromachined components. Applying various laser micromachining methods utilizing optimal parameters for each material can effectively control such barriers.

REFERENCES

[1] M.J. Madou, Fundamentals of Microfabrication and Nanotechnology, vol. II, CRC Press, Boca Raton, FL, 2011.
[2] S.Z. Chavoshi, X. Luo, Hybrid micro-machining processes: a review, Precis. Eng. 41 (2015) 1–23.
[3] M. Mehrpouya, H. Bidsorkhi, MEMS applications of NiTi based shape memory alloys: a review, Micro Nanosyst. 1 (8) (2016) 1–14.
[4] X. Luo, K. Cheng, D. Webb, F. Wardle, Design of ultraprecision machine tools with applications to manufacture of miniature and micro components, J. Mater. Process. Technol. 167 (2–3) (2005) 515–528.
[5] H. Lavvafi, J. Lewandowski, J. Lewandowski, Flex bending fatigue testing of wires, foils, and ribbons, Mater. Sci. Eng. A 601 (2014) 123–130.
[6] N. Muhammad, D. Whitehead, A. Boor, L. Li, Comparison of dry and wet fibre laser profile cutting of thin 316L stainless steel tubes for medical device applications, J. Mater. Process. Technol. 210 (15) (2010) 2261–2267.
[7] A.N. Samant, N.B. Dahotre, Laser machining of structural ceramics—a review, J. Eur. Ceram. Soc. 29 (6) (2009) 969–993.
[8] J.F. Ready, D.F. Farson, T. Feeley, LIA Handbook of Laser Materials Processing, Springer-Verlag, Berlin; Heidelberg, 2001.
[9] R.D. Schaeffer, Fundamentals of Laser Micromachining, CRC Press, Boca Raton, FL, 2012.
[10] J. Lawrence, J. Pou, D.K.Y. Low, E. Toyserkani, Advances in Laser Materials Processing: Technology, Research and Applications, Woodhead Publishing Limited, Cornwall, UK, 2010.
[11] J. Perriere, E. Millon, E. Fogarassy, Recent Advances in Laser Processing of Materials, Elsevier Ltd, Oxford, UK, 2006.
[12] D. Bäuerle, Laser Processing and Chemistry, Springer-Verlag, Berlin; Heidelberg, 2011.
[13] W.M. Steen, J. Mazumder, Laser Material Processing, Springer-Verlag, London, 2010.
[14] J. Krüger, W. Kautek, The femtosecond pulse laser: a new tool for micromachining, Laser Phys. 9 (1) (1999) 30–40.
[15] J. Ion, Laser Processing of Engineering Materials: Principles, Procedure and Industrial Application, Butterworth-Heinemann, Oxford, UK, 2005.
[16] P. Schaaf, Laser Processing of Materials: Fundamentals, Applications and Developments, Springer-Verlag, Berlin; Heidelberg, 2010.
[17] J. Dutta Majumdar, I. Manna, Laser material processing, Int. Mater. Rev. 56 (5-6) (2011) 341–388.
[18] T. Häfner, J. Heberle, M. Dobler, M. Schmidt, Influences on incubation in ps laser micromachining of steel alloys, J. Laser Appl. 28 (2) (2016) 022605.
[19] M. Olbrich, E. Punzel, P. Lickschat, S. Weißmantel, A. Horn, Investigation on the ablation of thin metal films with femtosecond to picosecond-pulsed laser radiation, Phys. Procedia 83 (2016) 93–103.
[20] K.C. Phillips, H.H. Gandhi, E. Mazur, S. Sundaram, Ultrafast laser processing of materials: a review, Adv. Opt. Photon. 7 (4) (2015) 684–712.
[21] W. Hu, Y.C. Shin, G.B. King, Micromachining of metals, alloys, and ceramics by picosecond laser ablation, J. Manuf. Sci. Eng. 132 (1) (2010) 011009.

[22] D.S. Correa, J.M. Almeida, G.F. Almeida, M.R. Cardoso, L. De Boni, C.R. Mendonça, Ultrafast laser pulses for structuring materials at micro/nano scale: from waveguides to superhydrophobic surfaces, Photonics 4 (1) (2017) 8.
[23] H. Lavvafi, D. Dudzinski, M. Young, J. Gbur, J.R. Lewandowski, J.J. Lewandowski, Parametric studies on femtosecond laser cutting of Ni-Ti shape memory alloy, in: Proc. MS&T 2012 Next Generation Biomaterials Symposium, 2012.
[24] A. Kuar, B. Doloi, B. Bhattacharyya, Modelling and analysis of pulsed Nd:YAG laser machining characteristics during micro-drilling of zirconia (ZrO 2), Int. J. Mach. Tools Manuf. 46 (12–13) (2006) 1301–1310.
[25] E. Chryssolouris, Laser Machining: Theory and Practice, Springer-Verlag, New York, NY, 1991.
[26] A.K. Dubey, V. Yadava, Experimental study of Nd: YAG laser beam machining—an overview, J. Mater. Process. Technol. 195 (1–3) (2008) 15–26.
[27] A. Riveiro, F. Quintero, F. Lusquiños, R. Comesaña, J. Pou, Influence of assist gas nature on the surfaces obtained by laser cutting of Al–Cu alloys, Surf. Coat. Technol. 205 (7) (2010) 1878–1885.
[28] A. Gisario, M. Mehrpouya, S. Venettacci, A. Mohammadzadeh, M. Barletta, LaserOrigami (LO) of three-dimensional (3D) components: experimental analysis and numerical modelling, J. Manuf. Process. 23 (2016) 242–248.
[29] A. Gisario, M. Mehrpouya, S. Venettacci, M. Barletta, Laser-assisted bending of Titanium Grade-2 sheets: experimental analysis and numerical simulation, Opt. Lasers Eng. 92 (2017) 110–119.
[30] A. Sharma, V. Yadava, Optimization of cut quality characteristics during Nd: YAG laser straight cutting of Ni-based superalloy thin sheet using grey relational analysis with entropy measurement, Mater. Manuf. Process. 26 (12) (2011) 1522–1529.
[31] A. Sharma, V. Yadava, Modelling and optimization of cut quality during pulsed Nd: YAG laser cutting of thin Al-alloy sheet for straight profile, Opt. Lasers Technol. 44 (1) (2012) 159–168.
[32] A. Sharma, V. Yadava, R. Rao, Optimization of kerf quality characteristics during Nd: YAG laser cutting of nickel based superalloy sheet for straight and curved cut profiles, Opt. Lasers Eng. 48 (9) (2010) 915–925.
[33] D.K. Das, T.M. Pollock, Femtosecond laser machining of cooling holes in thermal barrier coated CMSX4 superalloy, J. Mater. Process. Technol. 209 (15–16) (2009) 5661–5668.
[34] H. Lavvafi, Effects of laser machining on structure and fatigue of 316LVM biomedical wires, Ph.D. dissertation, Case Western Reserve University, 2013.
[35] S. Mishra, V. Yadava, Laser beam micromachining (LBMM)—a review, Opt. Lasers Eng. 73 (2015) 89–122.
[36] A. Pramanik, Developments in the non-traditional machining of particle reinforced metal matrix composites, Int. J. Mach. Tools Manuf. 86 (2014) 44–61.
[37] H. Booth, Recent applications of pulsed lasers in advanced materials processing, Thin Solid Films 453–454 (2004) 450–457.
[38] S. Zoppel, M. Farsari, R. Merz, J. Zehetner, G. Stangl, G.A. Reider, C. Fotakis, Laser micro machining of 3C–SiC single crystals, Microelectron. Eng. 83 (4–9) (2006) 1400–1402.
[39] M. Mehrpouya, S. Emamian, Recent advantages in laser fabrication of micro-channel heat exchangers, Mater. Werkst. 48 (2017) 205–209.
[40] J.C. Finlay, A. Darafsheh, Light sources, drugs, and dosimetry, in: B. Wong, J. Ilgner (Eds.), Biomedical Optics in Otorhinolaryngology: Head and Neck Surgery, Springer, New York, NY, 2016, pp. 311–336 (Chapter 19).
[41] B.E.A. Saleh, M.C. Teich, Fundamentals of Photonics, second ed., John Wiley & Sons, Hoboken, NJ, 2007.

[42] A.K. Dubey, V. Yadava, Multi-objective optimization of Nd: YAG laser cutting of nickel-based superalloy sheet using orthogonal array with principal component analysis, Opt. Lasers Eng. 46 (2) (2008) 124–132.
[43] J.D. Majumdar, I. Manna, Laser processing of materials, Sadhana 28 (3-4) (2003) 495–562.
[44] R. Rao, V. Yadava, Multi-objective optimization of Nd: YAG laser cutting of thin superalloy sheet using grey relational analysis with entropy measurement, Opt. Lasers Technol. 41 (8) (2009) 922–930.
[45] A.K. Dubey, V. Yadava, Optimization of kerf quality during pulsed laser cutting of aluminium alloy sheet, J. Mater. Process. Technol. 204 (1–3) (2008) 412–418.
[46] A.K. Pandey, A.K. Dubey, Simultaneous optimization of multiple quality characteristics in laser cutting of titanium alloy sheet, Opt. Lasers Technol. 44 (6) (2012) 1858–1865.
[47] C. Wang, X. Zeng, Study of laser carving three-dimensional structures on ceramics: quality controlling and mechanisms, Opt. Lasers Technol. 39 (7) (2007) 1400–1405.
[48] H. Lavvafi, M.E. Lewandowski, D. Schwam, J.J. Lewandowski, Effects of surface laser treatments on microstructure, tension, and fatigue behavior of AISI 316LVM biomedical wires, Mater. Sci. Eng. A 688 (14) (2017) 101–113.
[49] S. Gräf, G. Staupendahl, A. Krämer, F.A. Müller, High precision materials processing using a novel Q-switched CO_2 laser, Opt. Lasers Eng. 66 (2015) 152–157.
[50] A. Riveiro, F. Quintero, F. Lusquinos, R. Comesana, J. Pou, Parametric investigation of CO_2 laser cutting of 2024-T3 alloy, J. Mater. Process. Technol. 210 (9) (2010) 1138–1152.
[51] D. Basting, Excimer Laser Technology, Springer, Berlin, Heidelberg, 2005.
[52] N. Jebbari, M.M. Jebari, F. Saadallah, A. Tarrats-Saugnac, R. Bennaceur, J.P. Longuemard, Thermal affected zone obtained in machining steel XC42 by high-power continuous CO_2 laser, Opt. Lasers Technol. 40 (6) (2008) 864–873.
[53] R. Osellame, G. Cerullo, R. Ramponi, Femtosecond Laser Micromachining: Photonic and Microfluidic Devices in Transparent Materials, Springer, Berlin, Heidelberg, 2012.
[54] R. Mayerhofer, D. Mairhoermann, M. Mueller, Fiber lasers boost medical device production, Industr. Laser Solut. Manuf. 27 (3) (2012) 20.
[55] L. Cerami, E. Mazur, S. Nolte, C.B. Schaffer, Femtosecond laser micromachining, in: R. Thomson, C. Leburn, D. Reid (Eds.), Ultrafast Nonlinear Optics, Springer International Publishing, Cham, Switzerland, 2013, pp. 287–321.
[56] Q. Bian, X. Yu, B. Zhao, Z. Chang, S. Lei, Femtosecond laser ablation of indium tin-oxide narrow grooves for thin film solar cells, Opt. Lasers Technol. 45 (2013) 395–401.
[57] P. Bado, W. Clark, A. Said, Micromachining Handbook, Clark-MXR, Inc., Ann Arbor, MI, 2001.
[58] R.R. Gattass, E. Mazur, Femtosecond laser micromachining in transparent materials, Nat. Photonics 2 (4) (2008) 219–225.
[59] K.-H. Leitz, B. Redlingshöfer, Y. Reg, A. Otto, M. Schmidt, Metal ablation with short and ultrashort laser pulses, Phys. Procedia 12 (2011) 230–238.
[60] R. Viskup, High Energy and Short Pulse Lasers, InTech, Rijeka, Croatia, 2016.
[61] F. Korte, S. Nolte, B. Chichkov, T. Bauer, G. Kamlage, T. Wagner, C. Fallnich, H. Welling, Far-field and near-field material processing with. femtosecond laser pulses, Appl. Phys. A 69 (1) (1999) S7–S11.
[62] G.N. Makarov, Laser applications in nanotechnology: nanofabrication using laser ablation and laser nanolithography, Physics-Uspekhi 56 (7) (2013) 643–682.
[63] A.C. Tanous, Laser cutting takes the heat out of stent manufacturing, Industr. Laser Solut. Manuf. 25 (1) (2010) 20.
[64] M. Mielke, D. Gaudiosi, K. Kim, M. Greenberg, X. Gu, R. Cline, X. Peng, M. Slovick, N. Allen, M. Manning, M. Ferrel, N. Prachayaamorn, S. Sapers, Ultrafast fiber laser platform for advanced materials processing, J. Laser Micro/Nanoeng. 5 (1) (2010) 53–58.

[65] C.-H. Hung, F.-Y. Chang, Curve micromachining on the edges of nitinol biliary stent by ultrashort pulses laser, Opt. Lasers Technol. 90 (2017) 1–6.
[66] C.-H. Hung, F.-Y. Chang, T.-L. Chang, Y.-T. Chang, K.-W. Huang, P.-C. Liang, Micromachining NiTi tubes for use in medical devices by using a femtosecond laser, Opt. Lasers Eng. 66 (2015) 34–40.
[67] A. Darafsheh, Optical super-resolution and periodical focusing effects by dielectric microspheres, . Ph.D. dissertation, University of North Carolina at Charlotte, 2013.
[68] A. Darafsheh, Comment on 'Super-resolution microscopy by movable thin-films with embedded microspheres: Resolution analysis' [Ann. Phys. (Berlin) 527, 513 (2015)], Ann. Phys. (Berlin) 528 (11–12) (2016) 898–900.
[69] A. Darafsheh, C. Guardiola, A. Palovcak, J.C. Finlay, A. Cárabe, Optical super-resolution imaging by high-index microspheres embedded in elastomers, Opt. Lett. 40 (1) (2015) 5–8.
[70] A. Darafsheh, Influence of the background medium on imaging performance of microsphere-assisted super-resolution microscopy, Opt. Lett. 42 (4) (2017) 735–738.
[71] D. Araujo, F. Carpio, D. Mendez, A. Garcıa, M. Villar, R. Garcıa, D. Jimenez, L. Rubio, Microstructural study of CO_2 laser machined heat affected zone of 2024 aluminum alloy, Appl. Surf. Sci. 208–209 (2003) 210–217.
[72] N. Muhammad, B.D. Rogers, L. Li, Understanding the behaviour of pulsed laser dry and wet micromachining processes by multi-phase smoothed particle hydrodynamics (SPH) modelling, J. Phys. D. Appl. Phys. 46 (9) (2013) 095101.
[73] J. Dowden, The theory of laser materials processing: heat and mass transfer in modern technology, Springer, Dordrecht, The Netherlands, 2009.
[74] T. Kurita, T. Yamane, K. Ashida, S. Sasaki, Proposal for small heat-affected zone, high aspect ratio processing for metal, J. Mater. Process. Technol. 242 (2017) 228–234.
[75] T. Kurita, K. Komatsuzaki, M. Hattori, Advanced material processing with nano-and femto-second pulsed laser, Int. J. Mach. Tools Manuf. 48 (2) (2008) 220–227.
[76] D. Liu, J. Cheng, W. Perrie, A. Baum, P. Scully, M. Sharp, S. Edwardson, Z. Kuang, N. Semaltianos, P. French, G. Dearden, L. Li, K.G. Watkins, Femtosecond laser microstructuring of materials in the NIR and UV regime, in: Proc. 26th International Congress on Applications of Lasers and Electro-Optics (ICALEO'07), 2007, pp. 12–18.
[77] N.B. Dahotre, S. Harimkar, Laser fabrication and machining of materials, Springer, New York, NY, 2008.
[78] A. Grajcar, M. Różański, S. Stano, A. Kowalski, Microstructure characterization of laser-welded Nb-microalloyed silicon-aluminum TRIP steel, J. Mater. Eng. Perform. 23 (9) (2014) 3400–3406.
[79] L. Li, M. Sobih, P. Crouse, Striation-free laser cutting of mild steel sheets, CIRP Ann. Manuf. Technol. 56 (1) (2007) 193–196.
[80] N. Grabow, M. Schlun, K. Sternberg, N. Hakansson, S. Kramer, K.-P. Schmitz, Mechanical properties of laser cut poly (L-lactide) micro-specimens: implications for stent design, manufacture, and sterilization, J. Biomech. Eng. 127 (1) (2005) 25–31.
[81] P.R. Miller, R. Aggarwal, A. Doraiswamy, Y.J. Lin, Y.-S. Lee, R.J. Narayan, Laser micromachining for biomedical applications, JOM J. Miner. Met. Mater. Soc. 61 (9) (2009) 35–40.
[82] S.D. Gittard, R.J. Narayan, Laser direct writing of micro-and nano-scale medical devices, Expert Rev. Med. Devices 7 (3) (2010) 343–356.
[83] K. Sugioka, Y. Cheng, Ultrafast lasers—reliable tools for advanced materials processing, Light Sci. Appl. 3 (4) (2014) e149.
[84] C. Momma, U. Knop, S. Nolte, Laser cutting of slotted tube coronary stents, state of the art and future developments, Prog. Biomed. Res. 4 (1) (1999) 39–44.
[85] N. Muhammad, L. Li, Underwater femtosecond laser micromachining of thin nitinol tubes for medical coronary stent manufacture, Appl. Phys. A 107 (4) (2012) 849–861.

[86] M.F. Teixeira, V.A.V. Schmachtenberg, G. Tontini, G.D.L. Semione, W.L. Weingaertner, V. Drago, Laser composite surfacing of A681 steel with WC + Cr + Co for improved wear resistance, J. Mater. Res. Technol. 6 (1) (2017) 33–39.
[87] J. Zhang, T. Lee, X. Ai, W. Lau, Investigation of the surface integrity of laser-cut ceramic, J. Mater. Process. Technol. 57 (3-4) (1996) 304–310.
[88] S. Dauer, A. Ehlert, S. Büttgenbach, Rapid prototyping of micromechanical devices using a Q-switched Nd:YAG laser with optional frequency doubling, Sensors Actuators A Phys. 76 (1–3) (1999) 381–385.
[89] A.K. Dubey, V. Yadava, Laser beam machining—a review, Int. J. Mach. Tools Manuf. 48 (6) (2008) 609–628.
[90] M. Różański, M. Morawiec, A. Grajcar, S. Stano, Modified twin-spot laser welding of complex phase steel, Arch. Metall. Mater. 61 (4) (2016) 1999–2008.
[91] S. Stano, A. Grajcar, Z. Wilk, M. Różański, P. Matter, M. Morawiec, Microstructural aspects of twin-spot laser welding of dp-Hsla steel sheet joints, Arch. Metall. Mater. 61 (2) (2016) 731–740.
[92] Z. Xue, S. Hu, J. Shen, D. Zuo, E. Kannatey-Asibu Jr., Microstructure characterization and mechanical properties of laser-welded copper and aluminum lap joint, J. Laser Appl. 26 (1) (2014) 012002.
[93] H.N. Moosavy, M.-R. Aboutalebi, S.H. Seyedein, C. Mapelli, Microstructural, mechanical and weldability assessments of the dissimilar welds between γ′-and γ″-strengthened nickel-base superalloys, Mater. Charact. 82 (2013) 41–49.
[94] M. Pang, G. Yu, H.-H. Wang, C.-Y. Zheng, Microstructure study of laser welding cast nickel-based superalloy K418, J. Mater. Process. Technol. 207 (1–3) (2008) 271–275.
[95] R.I. Stephens, A. Fatemi, R.R. Stephens, H.O. Fuchs, Metal Fatigue in Engineering, John Wiley & Sons, Inc, New York, 2000.
[96] O.A. Zeid, On the effect of electrodischarge machining parameters on the fatigue life of AISI D6 tool steel, J. Mater. Process. Technol. 68 (1) (1997) 27–32.
[97] A. Medvedeva, J. Bergström, S. Gunnarsson, Inclusions, stress concentrations and surface condition in bending fatigue of an H13 tool steel, Steel Res. 79 (5) (2008) 376–381.
[98] J. Gbur, J. Lewandowski, Fatigue and fracture of wires and cables for biomedical applications, Int. Mater. Rev. 61 (4) (2006) 231–314.
[99] X. Wang, G. Ng, Z. Liu, L. Li, L. Bradley, EPMA microanalysis of recast layers produced during laser drilling of type 305 stainless steel, Thin Solid Films 453–454 (2004) 84–88.
[100] F. Yan, S. Liu, C. Hu, C. Wang, X. Hu, Liquation cracking behavior and control in the heat affected zone of GH909 alloy during Nd:YAG laser welding, J. Mater. Process. Technol. 244 (2017) 44–50.
[101] C. Karatas, O. Keles, I. Uslan, Y. Usta, Laser cutting of steel sheets: Influence of workpiece thickness and beam waist position on kerf size and stria formation, J. Mater. Process. Technol. 172 (1) (2006) 22–29.
[102] L. Shanjin, W. Yang, An investigation of pulsed laser cutting of titanium alloy sheet, Opt. Lasers Eng. 44 (10) (2006) 1067–1077.
[103] D. Jahns, T. Kaszemeikat, N. Mueller, D. Ashkenasi, R. Dietrich, H. Eichler, Laser trepanning of stainless steel, Phys. Procedia 41 (2013) 630–635.
[104] X. Wang, G. Ng, Z. Liu, L. Li, P. Skeldon, L. Bradley, Corrosion performance of recast layers produced during laser drilling of type 305 stainless steel, J. Corros. Sci. Eng. 6 (2003). Paper C123.
[105] B.T. Rao, R. Kaul, P. Tiwari, A. Nath, Inert gas cutting of titanium sheet with pulsed mode CO_2 laser, Opt. Lasers Eng. 43 (12) (2005) 1330–1348.